ORNL-TM-2812

Contract No. W-7405-eng-26

Reactor Division

A VISCOELASTIC REPRESENTATION OF THE MECHANICAL BEHAVIOR OF RVD GRAPHITE AT ELEVATED TEMPERATURES

C. E. Pugh

FEBRUARY 1970

OAK RIDGE NATIONAL LABORATORY
Oak Ridge, Tennessee
operated by
UNION CARBIDE CORPORATION
for the
U.S. ATOMIC ENERGY COMMISSION

DISCLAIMER

Contents

This page left intentionally blank

List of Symbols

A_i	Transient creep coefficients
E	Elastic modulus
$G_{ijkl}(t)$	Relaxation functions
$H(t)$	Heaviside step function
$J_{ijkl}(t)$	Creep compliance functions
R	Real gas constant
t	Time
T	Absolute temperature
U	Activation energy
x_i	Rectangular Cartesian coordinates
ϵ_{ij}	Strain components
σ_{ij}	Stress components
μ_{ij}	Strain ratios
η	Steady-state creep coefficient
τ_i	Retardation times

A VISCOELASTIC REPRESENTATION OF THE MECHANICAL BEHAVIOR OF RVD GRAPHITE AT ELEVATED TEMPERATURES

C. E. Pugh

Abstract

A set of constitutive equations is developed to describe the time-dependent mechanical behavior of RVD graphite at temperatures ranging from 3500 to 5000°F. The relations are based upon a transversely isotropic linear viscoelastic model with temperature-dependent parameters. This model is shown to be applicable for stress levels up to one-half the nominal ultimate stress values for the material and is expressed quantitatively through the use of experimental results. Predictions of these equations are compared with other experimental measurements including those from short-time stress-strain tests, creep tests, and relaxation tests.

Keywords: RVD graphite, transversely isotropic, viscoelastic, constitutive equations, stress, strain, temperature, time, creep, relaxation.

Introduction

Studies of time-dependent behaviors of various nuclear-grade graphites over a range of elevated temperatures have been reported by numerous authors. Many of these investigations are discussed by Reynolds[1†] and by Greenstreet.[2] The reported studies have generally addressed themselves only to the mathematical representation of the response of a given material to a single type of mechanical loading, such as uniaxial creep, relaxation, or recovery. The literature contains very little information about efforts to develop complete sets of constitutive equations applicable to these conditions or about efforts to verify representations through comparisons of analytical predictions with experimental results for tests other than those used in the development of models.

---

†Superscript numbers refer to similarly numbered references at the end of this report.

This paper presents a unified mathematical characterization of the mechanical behavior of RVD graphite for temperatures ranging from 3500 to 5000°F. A set of temperature-dependent constitutive equations applicable over this temperature range is developed to describe the mechanical response of the material to general loadings. Experimental results are used in both parameter evaluation and in verification of mathematical models.

Within this temperature range, creep and relaxation mechanisms for graphite are operative and give rise to a mechanical behavior which is both time and temperature dependent. A transversely isotropic linear viscoelastic model is shown to characterize this mechanical behavior over a limited stress range.

First, the forms of the constitutive equations representing a transversely isotropic linear viscoelastic model are formulated in terms of hereditary integrals which contain five independent material properties — three strain ratios and two creep functions. The three strain ratios are assumed independent of time, stress, and strain, but are temperature dependent. Thus, the time-dependent character of the mechanical behavior is accounted for by two creep functions.

The experimental data used in this study include the results of a larger number of tests performed at 4500°F than any other temperature. Therefore, the parameters appearing in the constitutive equations are first evaluated at that temperature. Only data from with-grain and across-grain tensile tests and from with-grain creep tests are used in this evaluation. A temperature dependence is then introduced into the model by also considering data from with-grain tensile and creep tests conducted at 3500, 4000, and 5000°F.

The constitutive equations developed in this manner are then used to predict the results of tests other than those used for evaluation of parameters. Consequently, the correlation of these predictions with experimental measurements indicates the capability of this model to predict the mechanical response of RVD graphite to more general loadings in this temperature range.

Characterization of Material Behavior

RVD is a fine-grain nuclear-grade graphite with a maximum particle size of 0.015 in. It is also a molded graphite and, consequently, has material properties which are orientation dependent. However, the material properties are essentially independent of orientation within planes perpendicular to the molding direction. These planes are considered to be planes of mechanical isotropy and directions parallel to these planes are referred to as with-grain directions. Consequently, the direction normal to these planes, the molding direction, is referred to as the across-grain direction. This type of material symmetry defines a transversely isotropic material and places restrictions on the forms of the constitutive equations to be subsequently presented.

The experimental program utilized in this study has been described in detail by Woodard.[3] This experimental program included various uniaxial tests conducted as constant stress creep tests, stress relaxation tests, and short-time constant strain-rate tests. These tests were performed with both with-grain and across-grain specimens at four specific temperatures — 3500, 4000, 4500, and 5000°F.

In this temperature range, deformation mechanisms are operative in RVD graphite which make mechanical processes time dependent. This is illustrated for 4500°F by Fig. 1 which shows creep strains as functions of time for several individual with-grain specimens which were subjected to constant uniaxial stress values. The stress level for each test is indicated in psi by the number adjacent to the corresponding creep curve. The indicated stress levels range up to approximately 75% of the nominal with-grain ultimate strength for this temperature.

The dependence of these creep curves upon the stress level is investigated by plotting the ratio of creep strain per unit stress, which corresponds to a given creep time, versus stress. For example, this type of plot which corresponds with t = 20 minutes for the creep tests shown in Fig. 1 is given in Fig. 2. This plot shows the ratio of with-grain creep strain to stress to be, within reasonable experimental scatter, constant with stress up to 3700 psi at 4500°F. This stress level is

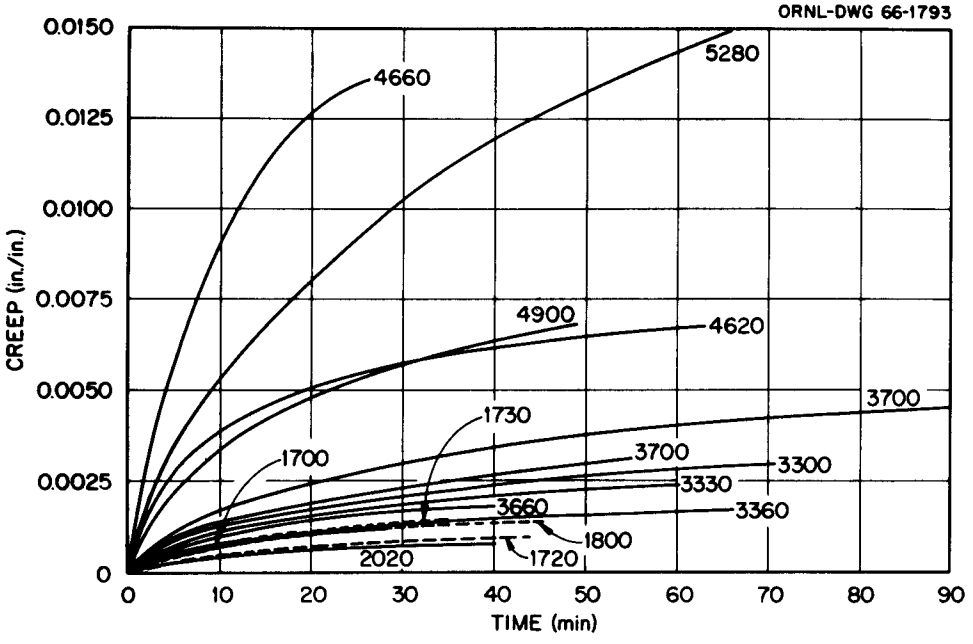

Fig. 1. With-Grain Tensile Creep at 4500°F.

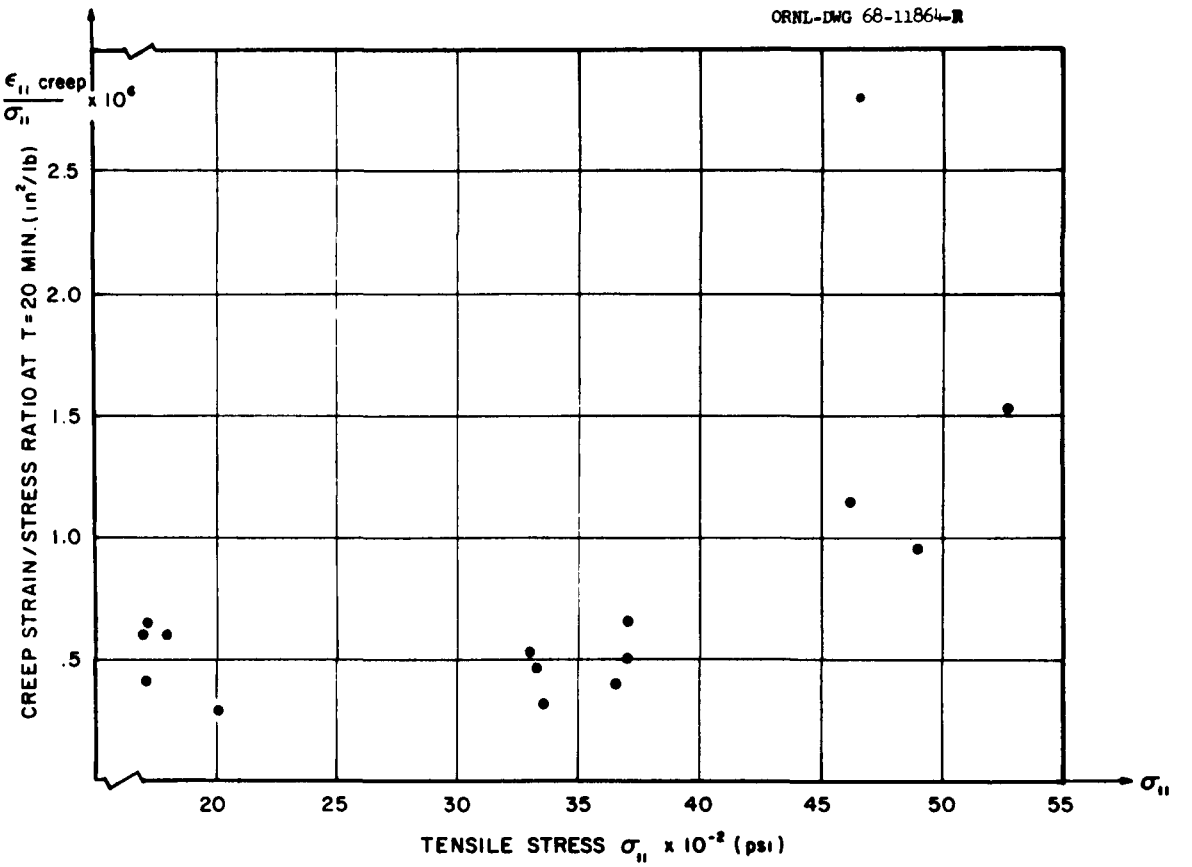

Fig. 2. With-Grain Creep Strain/Stress Versus Stress at 4500°F.

approximately 50% of the nominal ultimate stress value for the with-grain direction of RVD graphite at 4500°F.

A similar dependence of the creep strain upon the stress level was observed at the other test temperatures. Therefore, for stress levels up to 50% of the nominal ultimate stress value, the creep strains have an approximately linear dependence upon the stress level. Beyond this stress level, the dependence is clearly nonlinear.

These observations suggest that the mechanical behavior of this material can be characterized by a transversely isotropic linear viscoelastic model for this limited stress range. The model is considered to be temperature dependent, and the limiting stress value, below which the model is considered to be applicable, is taken to be one-half the nominal ultimate stress value corresponding to the given temperature. Therefore, for both parameter evaluation and model verification, the only test results considered in this report are those from tests conducted at stress levels below this limiting stress.

Constitutive Equations

The time-dependent strains $\epsilon_{ij}(t)$, (i, j = 1, 2, 3), which result from successive stress increments $\Delta_1\sigma_{ij}$, $\Delta_2\sigma_{ij}$, ..., $\Delta_n\sigma_{ij}$ applied at times t_1, t_2, ..., t_n, respectively, to a linear viscoelastic material, are equal to the linear superposition of the strains which would correspond to each stress increment if applied separately to the material. Therefore, the components of stress and strain are related in the following manner:*

$$\epsilon_{ij}(t) = \sum_{m=1}^{n} J_{ijkl}(t - t_m)\, \Delta_m\sigma_{kl} \ , \qquad (1)$$

where $J_{ijkl}(t)$ are creep compliance functions which characterize the time-dependent response of the material and t is the time at which the strains are evaluated. Therefore, as fully described by Flügge,[4] the strains which

*A repeated subscript implies summation of terms over the range one to three.

result from an arbitrary time-varying stress $\sigma_{kl}(t)$ are represented by

$$\epsilon_{ij}(t) = \int_o^t J_{ijkl}(t - \tau) \frac{\partial \sigma_{kl}}{\partial \tau} d\tau , \qquad (2)$$

where the integration variable τ ranges over the history of the loading program. The initial values of the creep functions, $J_{ijkl}(o)$, represent the elastic compliances.

Since RVD is characterized to be a transversely isotropic material, the constitutive equations, Eq. (2), must be expressed in a form which exhibits an axis of rotational symmetry. The plane of isotropy is defined, here, by the rectangular Cartesian coordinates (x_1, x_2), and the directions parallel to this plane are referred to as with-grain directions. The x_3 axis defines the direction normal to the plane of isotropy and is referred to as the across-grain direction.

As shown by Rogers and Pipkin,[5] there are only five components of $J_{ijkl}(t)$ which are independent of each other in the description of a transversely isotropic linear viscoelastic material. If the ratios of induced lateral strains to longitudinal strains for uniaxial states of stress are assumed to be independent of time, stress, and strain, then the constitutive equations for such a material at a constant temperature become

$$\epsilon_{11}(t) = \int_o^t J_{11}(t - \tau) \left[\frac{\partial \sigma_{11}}{\partial \tau} - \mu_{12} \frac{\partial \sigma_{22}}{\partial \tau} - \mu_{13} \frac{\partial \sigma_{33}}{\partial \tau}\right] d\tau ,$$

$$\epsilon_{22}(t) = \int_o^t J_{11}(t - \tau) \left[\frac{\partial \sigma_{22}}{\partial \tau} - \mu_{12} \frac{\partial \sigma_{11}}{\partial \tau} - \mu_{13} \frac{\partial \sigma_{33}}{\partial \tau}\right] d\tau ,$$

$$\epsilon_{33}(t) = \frac{\mu_{13}}{\mu_{31}} \int_o^t J_{11}(t - \tau) \left[\frac{\partial \sigma_{33}}{\partial \tau} - \mu_{31} \frac{\partial}{\partial \tau} (\sigma_{11} + \sigma_{22})\right] d\tau ,$$

$$\epsilon_{23}(t) = \frac{1}{2} \int_o^t J_{44}(t - \tau) \frac{\partial \sigma_{23}}{\partial \tau} d\tau ,$$

$$\epsilon_{13}(t) = \frac{1}{2} \int_o^t J_{44}(t - \tau) \frac{\partial \sigma_{13}}{\partial \tau} d\tau , \qquad (3)$$

[continued]

$$\epsilon_{12}(t) = (1 + \mu_{12}) \int_0^t J_{11}(t - \tau) \frac{\partial \sigma_{12}}{\partial \tau} \, d\tau \, , \tag{3}$$

where $J_{11}(t)$ and $J_{44}(t)$ are independent creep functions and μ_{ij} are the ratios of the lateral strains induced in the x_j directions to the longitudinal strains for a uniaxial stress applied in the x_i directions.

The inverse constitutive relations, which give stresses in terms of strains, can be found from Eqs. (3) through the use of Laplace transforms and have the forms

$$\begin{aligned}
\sigma_{11}(t) &= \beta \int_0^t G_{11}(t - \tau) \left[\frac{\partial \epsilon_{11}}{\partial \tau} + \alpha_1 \frac{\partial \epsilon_{22}}{\partial \tau} + \alpha_2 \frac{\partial \epsilon_{33}}{\partial \tau} \right] d\tau \, , \\
\sigma_{22}(t) &= \beta \int_0^t G_{11}(t - \tau) \left[\frac{\partial \epsilon_{22}}{\partial \tau} + \alpha_1 \frac{\partial \epsilon_{11}}{\partial \tau} + \alpha_2 \frac{\partial \epsilon_{33}}{\partial \tau} \right] d\tau \, , \\
\sigma_{33}(t) &= \beta \int_0^t G_{11}(t - \tau) \left[\alpha_3 \frac{\partial \epsilon_{33}}{\partial \tau} + \alpha_2 \frac{\partial}{\partial \tau} (\epsilon_{11} + \epsilon_{22}) \right] d\tau \, , \\
\sigma_{23}(t) &= 2 \int_0^t G_{44}(t - \tau) \frac{\partial \epsilon_{23}}{\partial \tau} \, d\tau \, , \\
\sigma_{13}(t) &= 2 \int_0^t G_{44}(t - \tau) \frac{\partial \epsilon_{13}}{\partial \tau} \, d\tau \, , \\
\sigma_{12}(t) &= \beta(1 - \alpha_1) \int_0^t G_{11}(t - \tau) \frac{\partial \epsilon_{12}}{\partial \tau} \, d\tau \, ,
\end{aligned} \tag{4}$$

where $G_{11}(t)$ and $G_{44}(t)$ are independent relaxation functions and

$$\begin{aligned}
\alpha_1 &= \frac{\mu_{12} + \mu_{13} \mu_{31}}{1 - \mu_{13} \mu_{31}} \, , \\
\alpha_2 &= \frac{\mu_{31} (1 + \mu_{12})}{1 - \mu_{13} \mu_{31}} \, ,
\end{aligned} \tag{5}$$

[continued]

$$\alpha_3 = \frac{\mu_{31}\,(1 - \mu_{12}^2)}{\mu_{13}\,(1 - \mu_{13}\,\mu_{31})}\,,$$

$$\beta = \frac{1}{(1 - \mu_{12}\,\alpha_1 - \mu_{13}\,\alpha_2)}\,. \tag{5}$$

The relaxation functions are related to the creep functions by

$$\int_0^t J_{11}(t - \tau)\, G_{11}(\tau)\, d\tau = t\, H(t)$$

and (6)

$$\int_0^t J_{44}(t - \tau)\, G_{44}(\tau)\, d\tau = t\, H(t)\,,$$

where $H(t)$ is the Heaviside unit step function.

Five parameters, $J_{11}(t)$, $J_{44}(t)$, μ_{12}, μ_{13}, and μ_{31}, must be evaluated for the complete determination of these constitutive equations at a given temperature. In order to establish the constitutive equations over a range of temperatures, each of these five parameters is considered to be temperature dependent.

Evaluation of Material Parameters

The experimental data on which this study is based are sufficient for the complete determination of this model except for the creep function $J_{44}(t)$ which describes the shear behavior in planes normal to the plane of isotropy. This description is sufficient, however, to allow predictions for a wide variety of problems which do not involve this type of shear behavior. Among these are plane strain, plane stress, and axisymmetric problems, when in each case the defining plane is the plane of isotropy.

The strain ratios are determined as functions of temperature from short-time constant strain-rate tests. Direct measurements of μ_{12} and μ_{31} were made from tests conducted at 3500, 4000, 4500, and 5000°F. The average measured values for each of these two strain ratios were fitted, in the sense of least squares, by linear functions of the absolute

temperature (°R) and were expressed by

$$\mu_{12} = 0.31\ T \times 10^{-4} + 1.22 \times 10^{-2} \tag{7}$$

and

$$\mu_{31} = 0.266\ T \times 10^{-4} + 2.25 \times 10^{-2}\ . \tag{8}$$

Figure 3 shows a comparison of the average measured values for μ_{12} and μ_{31} and the values given by Eqs. (7) and (8).

The strain ratio μ_{13} is determined from μ_{31} by utilizing Eqs. (4) to show that the ratio of the stresses σ_{11} and σ_{33}, which corresponds to the same strain level for identical uniaxial loading programs in the x_1 and x_3 directions, respectively, assumes a constant value:

$$\frac{\sigma_{11}\ (\epsilon_{11} = \epsilon_o)}{\sigma_{33}\ (\epsilon_{33} = \epsilon_o)} = \frac{\mu_{13}}{\mu_{31}}\ . \tag{9}$$

Figure 3 shows a plot of this ratio versus temperature as determined from the average measured with-grain and across-grain stress-strain curves corresponding to constant strain-rate tests (0.02 min^{-1}). The values of this ratio for the various temperatures were found to be essentially independent of the strain level. A parabolic fit was obtained to these data and is also shown in Fig. 3. The resulting expression for the strain ratio μ_{13} is

$$\mu_{13} = 17.7\ T^3 \times 10^{-12} - 15.2\ T^2 \times 10^{-8} + 2.92\ T \times 10^{-4} + 0.366\ , \tag{10}$$

where T is the absolute temperature (°R).*

The uniaxial creep tests to be used in evaluating the creep function $J_{11}(t)$ were conducted by loading with-grain specimens to prescribed stress levels which were then held constant for up to 50 minutes. The loads were

---

*Due to the preferred orientation, the layer planes of the coke particles are parallel to the with-grain plane and possess a different chemical bonding mechanism from the interlayer, or across-grain, direction.[6] These different bonding mechanisms may explain why μ_{13} exhibits a distinctly different temperature dependence from either μ_{12} or μ_{31}, as only μ_{13} involves an induced strain in the across-grain direction.

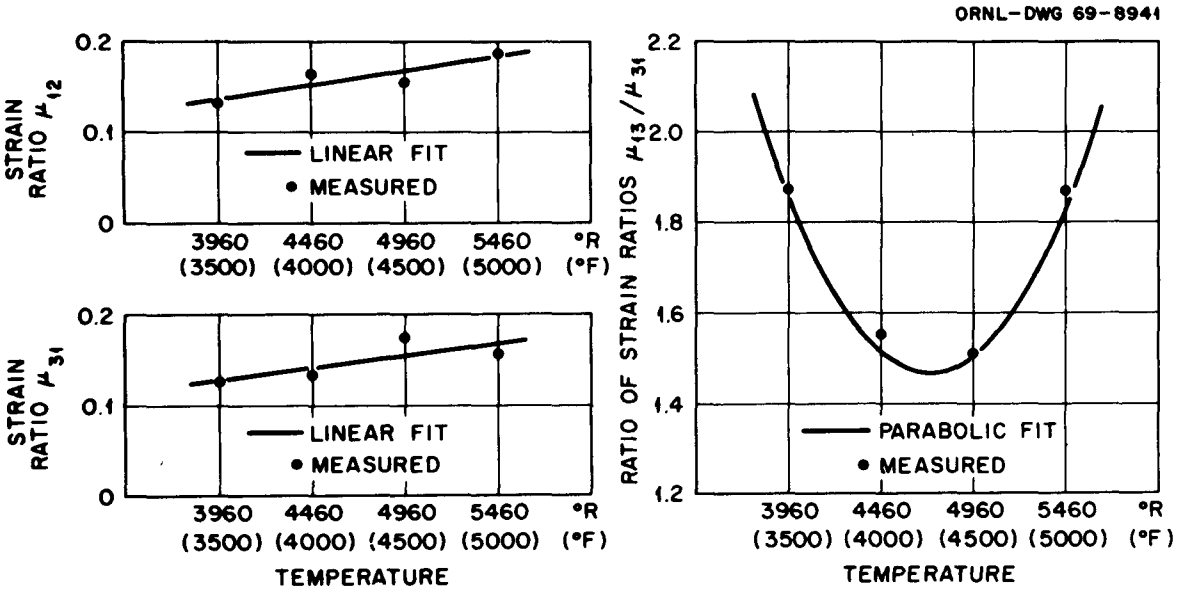

Fig. 3. Strain Ratios as Functions of Temperature.

applied to these specimens by extending them at a constant strain rate ($0.02\ \text{min}^{-1}$). Therefore, the values for the creep function, $J_{11}(t)$, during this brief loading time interval must be determined from constant strain-rate test data.

It can be shown from Eqs. (4) that for a constant strain-rate uniaxial loading program the relaxation function, $G_{11}(t)$, can be evaluated for the loading time interval from either with-grain or across-grain tests by the relations

$$G_{11}(t) = \frac{d\sigma_{11}}{d\epsilon_{11}} = \frac{\mu_{13}}{\mu_{31}} \frac{d\sigma_{33}}{d\epsilon_{33}} . \tag{11}$$

The average stress-strain curves for constant strain-rate ($0.02\ \text{min}^{-1}$) tests for across-grain specimens at the temperatures of interest were described by an equation due to Woolley[7] which has the form

$$\sigma_{33} = A\left(1 - e^{-k\epsilon_{33}}\right), \tag{12}$$

where A and k are material constants. For the specific constant strain rate of $\dot{\epsilon}_{33} = 0.02\ \text{min}^{-1}$, $\epsilon_{33}(t) = 0.02\ t$ and the relaxation function is given by Eqs. (11) and (12) to be

$$G_{11}(t) = \frac{\mu_{13}}{\mu_{31}} Ake^{-0.02\ kt} , \tag{13}$$

where t is measured in minutes. Equations (6) and (13) then give the creep function for this same limited time range as

$$J_{11}(t) = \frac{\mu_{13}}{\mu_{31}} \frac{1}{Ak} [1 + 0.02\ kt] . \tag{14}$$

If t* is the time required to reach the desired stress level for a uniaxial creep test in the with-grain direction, then $J_{11}(t)$ is given by Eq. (14) for $t \leq t^*$, and as can be shown from Eqs. (3) for $t > t^*$ by

$$J_{11}(t) = J_{11}(t^*) + \frac{\epsilon_{11}(t)_{creep}}{\sigma_{11}(t^*)} . \tag{15}$$

In Eq. (15), $\epsilon_{11}(t)_{creep}$ is the creep strain which has occurred from the time t* to the time t. The measured values used in Eq. (15) for $\epsilon_{11}(t)_{creep}/\sigma_{11}(t^*)$ correspond to the average creep per unit stress for all tests conducted at stress levels below one-half the nominal ultimate stress value. The value of t* is taken as the average time required to load these specimens to the desired stress levels by extending them at the prescribed constant strain rate ($0.02\ min^{-1}$).

The entire creep function, $J_{11}(t)$, is interpreted in terms of an elastic response, a viscous component, and a retarded elastic portion. At any given temperature, this description takes the mathematical form:

$$J_{11}(t) = \frac{1}{E} + \eta t + \sum_{i=1}^{3} A_i \left(1 - e^{-t/\tau_i}\right), \qquad (16)$$

where E, η, A_i, and τ_i are temperature-dependent material parameters.

Since the data used in this study include the results of more tests conducted at 4500°F than any other temperature, the creep function is first determined at this temperature. The first parameter, E, is taken as the initial slope of the with-grain stress-strain curve corresponding to constant strain-rate test ($0.02\ min^{-1}$) and the coefficient of the second term as the slope of the creep strain per unit stress versus time curve at the end of the data collection period (t = 50 minutes). The remaining three terms were fitted in the sense of least squares to the difference between $J_{11}(t)$ data and the two contributions mentioned above. The resulting expression for the creep function at 4500°F is

$$J_{11}(t) = \Big[0.467 + 0.0055\ t + 0.202\left(1 - e^{-19.49\ t}\right) + 0.109\left(1 - e^{-0.377\ t}\right) + 0.357\left(1 - e^{-0.0682\ t}\right)\Big]\ 10^{-6}\ (psi)^{-1}\ . \qquad (17)$$

Figure 4 illustrates the accuracy of this representation of $J_{11}(t)$ data by plotting the measured with-grain creep strain per unit stress values along with the results of Eqs. (15) and (17).

The creep function developed for T = 4500°F is taken as a reference function and a temperature dependence introduced such that at the other

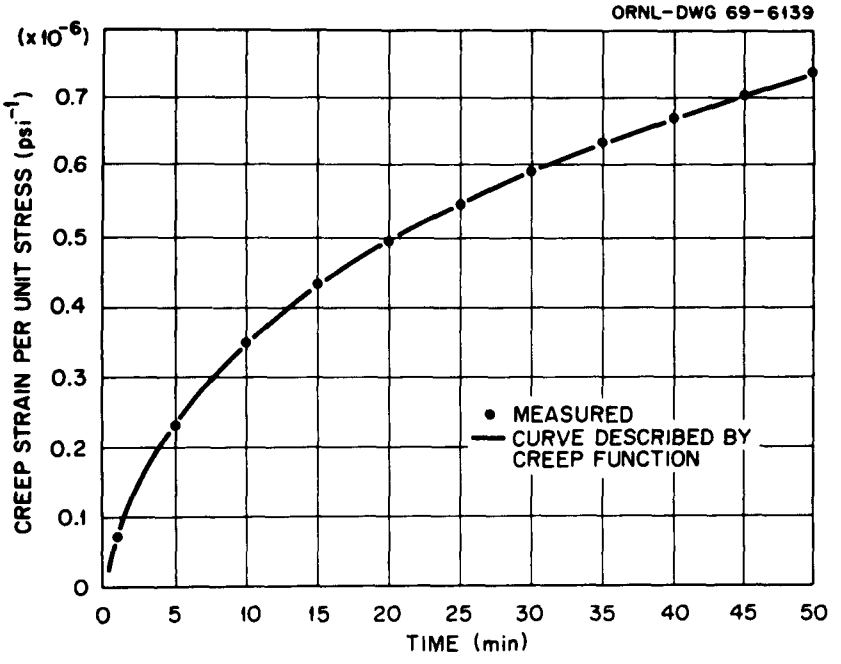

Fig. 4. RVD With-Grain Tensile Creep at 4500°F.

temperatures (3500, 4000, and 5000°F) the values given by the model for the initial modulus, for the duration of primary creep, and for the creep strain and creep strain rate at the end of the data collection periods for with-grain tests all agree with the respective experimental observations.

The temperature-dependent model developed in this manner was subsequently used to predict the across-grain creep behavior by the method outlined in the next section. At 3500°F considerable discrepancy was found between the model predictions and across-grain creep data. Therefore, in order to better represent the overall material behavior the model presented here requires the discrepancies between the model predictions and the average measured creep curves to be equal for both the with-grain and across-grain directions at 3500°F. With this modification, the resulting creep function is found to be

$$J_{11}(t,T) = \frac{\phi_o}{E} + A_1 \phi_1 \left(1 - e^{-\phi_3 t/\tau_1}\right) + \phi_2 \left[\eta\phi_4 t + A_2 \left(1 - e^{-\phi_3 t/\tau_2}\right) + A_3 \left(1 - e^{\phi_3 t/\tau_3}\right)\right], \quad (18)$$

where the ϕ's are functions of temperature and where E, η, A_i, and τ_i have the values given in Eq. (17). Specifically, the ϕ functions were determined to be

$$\begin{aligned}
\phi_o(T) &= 1.64\ T \times 10^{-4} + 0.186\ , \\
\phi_1(T) &= 37.67\ e^{-19.6 \times 10^3/RT}\ , \\
\phi_2(T) &= 2.32\ e^{-7.58 \times 10^3/RT} + 3.16 \times 10^{10}\ e^{-135.1 \times 10^3/RT}\ , \\
\phi_3(T) &= 63.47\ e^{-19.77 \times 10^3/RT} - 0.631\ , \\
\phi_4(T) &= 12.96 \times 10^6\ e^{-88.45 \times 10^3/RT}\ ,
\end{aligned} \quad (19)$$

where T is the absolute temperature in degrees Rankine and R is the universal gas constant. Since the reference creep function corresponds to 4500°F, all of the ϕ functions have the value of unity at that temperature.

Figures 5 and 6 show the comparison of the average measured with-grain creep per unit stress curves for T = 4000 and 5000°F, respectively, and

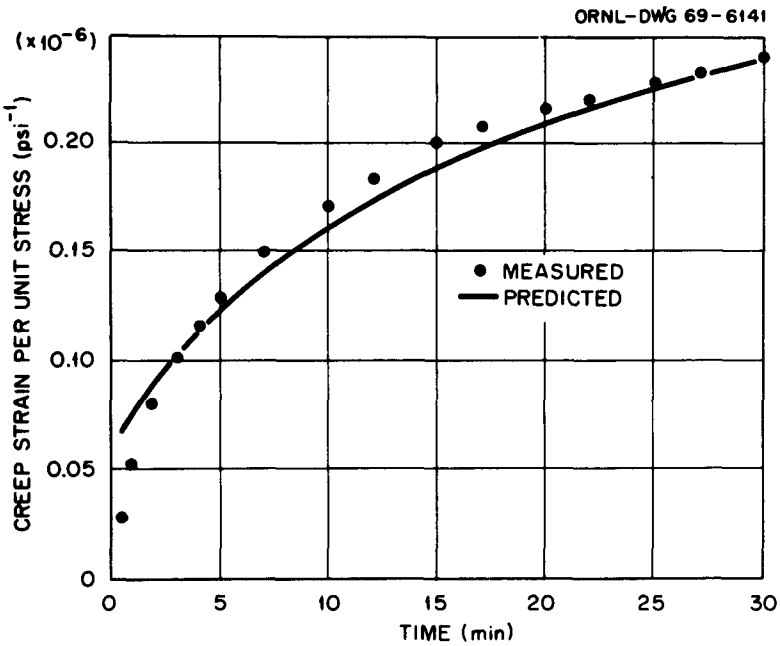

Fig. 5. RVD With-Grain Tensile Creep at 4000°F.

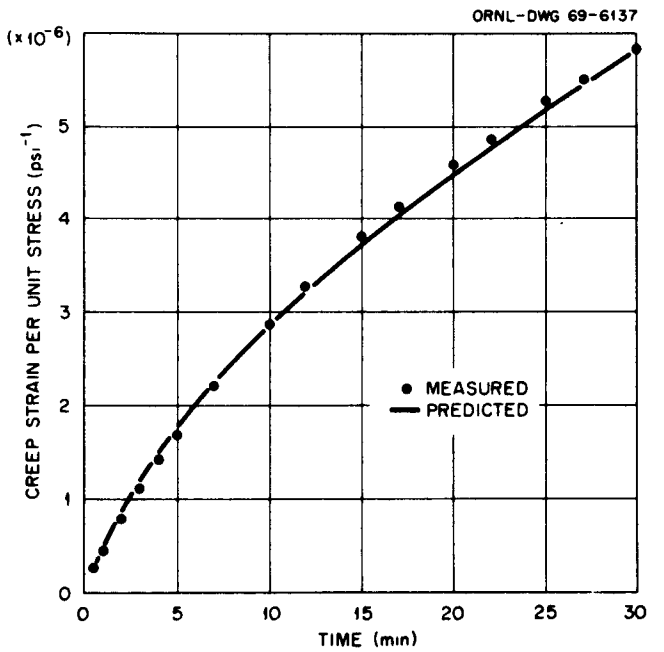

Fig. 6. RVD With-Grain Tensile Creep at 5000°F.

the predictions of the model described above. Figure 7 illustrates the comparisons of the model predictions with both the measured with-grain and across-grain creep per unit stress curves at 3500°F. As discussed earlier, it is seen that the discrepancies between the two predicted curves and the two measured curves are equal in magnitude. It should be pointed out that the creep rates at 3500°F are small in comparison with those at the highest temperatures studied. The actual discrepancy between the measured and predicted with-grain creep strain at t = 30 minutes is approximately 0.005% per 1000 psi. The experimental data shown in Figs. 5 through 7 correspond to the average creep strain per unit stress curves for tests conducted at stress levels below one-half the nominal ultimate stress values for the respective temperatures.

By considering the product of $\phi_2(T) \cdot \phi_4(T)$, a temperature-dependent activation energy is associated with the steady-state creep term. This is done by recognizing that if the temperature dependence of the steady-state creep coefficient could be characterized by a single activation energy, then this temperature dependence would be expressed as

$$\phi(T) = Ae^{-U/RT} . \tag{20}$$

It then follows that

$$U = \frac{-R}{\phi(T)} \frac{d\phi(T)}{d(1/T)} . \tag{21}$$

Using $\phi(T) = \phi_2(T) \cdot \phi_4(T)$ and Eqs. (19) in Eq. (21) gives rise to an effective activation energy which varies from 106 kcal/mole at 3500°F to 228 kcal/mole at 5000°F.

Comparison of Theory and Experiments

Using the viscoelastic model developed in the previous section, predictions are made of the mechanical response of RVD graphite to tests other than those used in the model development. Since experimental results of these tests were not used in parameter evaluations, they permit a completely independent comparison of model predictions and experimental measurements. First, predictions are made of the uniaxial creep response

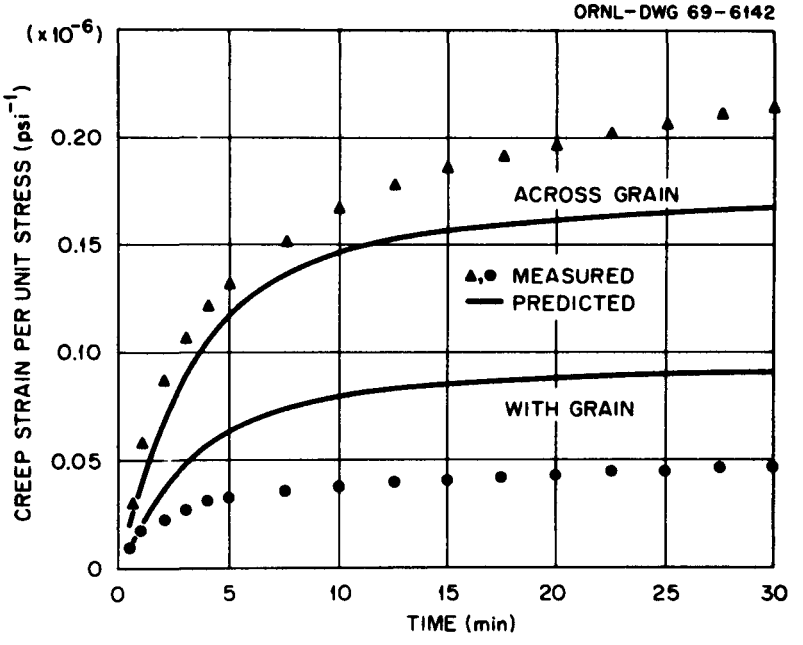

Fig. 7. RVD Tensile Creep at 3500°F.

of across-grain specimens. The constitutive equations, Eqs. (3), predict the across-grain creep strain per unit stress to be

$$\frac{\epsilon_{33}(t,T)_{creep}}{\sigma_{33}(t^*)} = \frac{\mu_{13}(T)}{\mu_{31}(T)} \left[J_{11}(t,T) - J_{11}(t^*,T)\right] , \qquad (22)$$

where t^* is the time required to load the specimen to the prescribed stress level, $\sigma_{33}(t^*)$. Figures 8 through 10 show the comparisons of these predictions with the respective average results of tests conducted at 4000, 4500, and 5000°F and at stress levels below one-half the respective nominal ultimate stress values. The loads were applied by extending the specimens at a constant strain rate (0.02 min^{-1}).

The constitutive equations are next used to predict the stress decay for both with-grain and across-grain relaxation tests performed at 4500°F. Experimental tests were performed by first extending uniaxial specimens at a constant strain rate (0.02 min^{-1}) to prescribed strain levels which corresponded to stress levels below one-half the nominal ultimate stress values. The strains were then held constant while the decreasing stresses were recorded. The constitutive equations, Eqs. (4), predict the stress per unit strain for with-grain and across-grain specimens loaded in this manner to be

$$\frac{\sigma_{11}(t)}{\epsilon_{11}(t_w^*)} = G_{11}(t) - G_{11}(t_w^*) + \frac{\sigma_{11}(t_w^*)}{\epsilon_{11}(t_w^*)}$$

and (23)

$$\frac{\sigma_{33}(t)}{\epsilon_{33}(t_a^*)} = \frac{\mu_{31}}{\mu_{13}} \left[G_{11}(t) - G_{11}(t_a^*)\right] + \frac{\sigma_{33}(t_a^*)}{\epsilon_{33}(t_a^*)} ,$$

respectively, where t_w^* and t_a^* are the times required to load with-grain and across-grain specimens, respectively, to the prescribed strain levels.

The relaxation function $G_{11}(t)$ for T = 4500°F is determined from Eqs. (6) and (17) through the use of Laplace transforms to be

$$G_{11}(t) = \Big(0.653\, e^{-27.98\, t} + 0.254\, e^{-0.446\, t} + 0.399\, e^{-0.101\, t} + 0.838\, e^{-0.00473\, t}\Big)\, 10^6 \text{ psi} . \qquad (24)$$

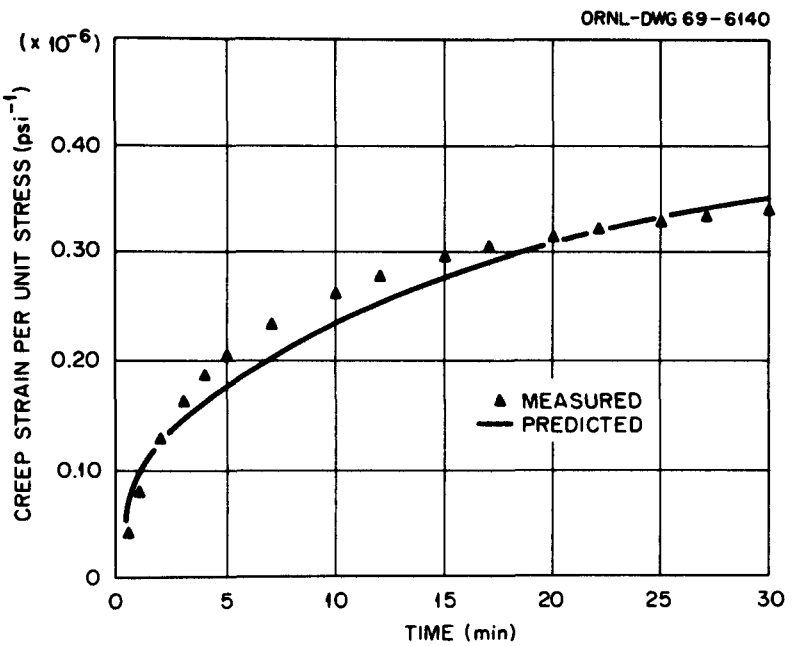

Fig. 8. RVD Across-Grain Tensile Creep at 4000°F.

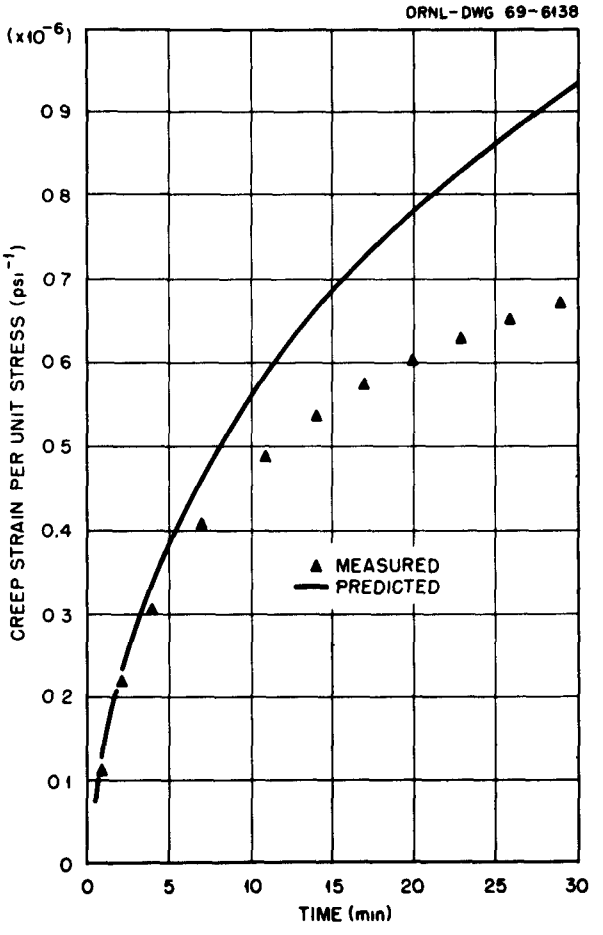

Fig. 9. RVD Across-Grain Tensile Creep at 4500°F.

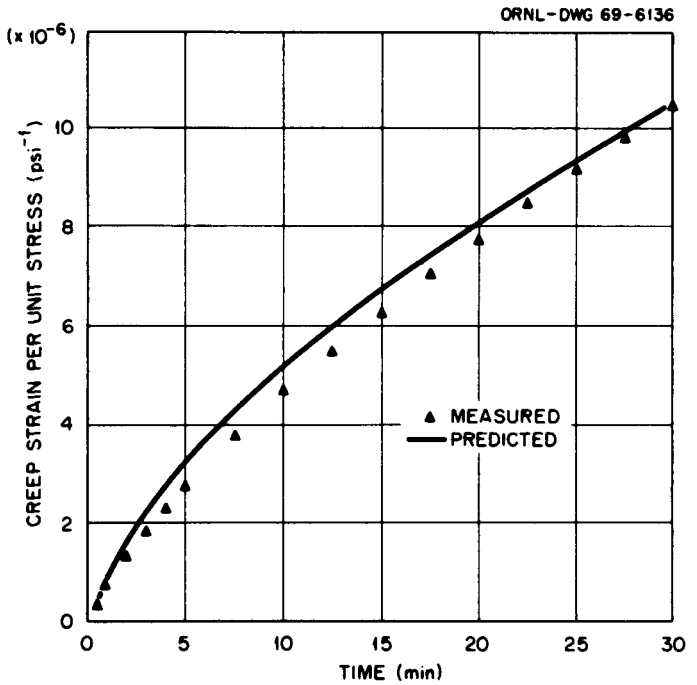

Fig. 10. RVD Across-Grain Tensile Creep at 5000°F.

Figure 11 shows the comparisons of the predictions of Eqs. (23) and (24) with the average experimental relaxation curves for both with-grain and across-grain specimens tested at 4500°F.

Stress-strain curves for both the with-grain and across-grain directions were determined by measurements from uniaxial constant strain-rate (0.02 min^{-1}) tensile tests at 3500, 4000, 4500, and 5000°F. The uniaxial stress-strain relations for with-grain and across-grain specimens extended at constant strain rates $\dot{\epsilon}_{xx}$ and $\dot{\epsilon}_{zz}$, respectively, are obtained from the constitutive equations as

$$\sigma_{xx}(t) = \dot{\epsilon}_{xx} \int_0^t G_{11}(t - \tau)\, d\tau$$

and (25)

$$\sigma_{zz}(t) = \frac{\mu_{31}}{\mu_{13}} \dot{\epsilon}_{zz} \int_0^t G_{11}(t - \tau)\, d\tau ,$$

respectively. The relaxation functions corresponding to the temperatures of interest are determined from Eqs. (6) and (18). Time is replaced in the integrated results of Eqs. (25) by $t = \epsilon_{xx}/\dot{\epsilon}_{xx}$ or $t = \epsilon_{zz}/\dot{\epsilon}_{zz}$ to yield the actual stress-strain relationships for these uniaxial tests. Figure 12 shows comparisons of the stress-strain curves predicted by using this temperature-dependent model with the average measured stress-strain curves. At all temperatures, the correlation between these two sets of curves for both the with-grain and across-grain directions is quite good for stress levels up to at least one-half the nominal ultimate stress. The final experimental points shown in Fig. 12 are in the vicinity of the average measured ultimate stress values.

In order to investigate the effects of strain rates on the stress-strain behavior of RVD graphite at 4500°F, with-grain uniaxial specimens were extended at three distinct strain rates (0.001, 0.02, and 0.10 min^{-1}). The strain-rate value has a pronounced effect on the stress-strain curve, as can be seen from Fig. 13. The resistance to deformation increases with increasing strain rate. The stress-strain curves predicted by the analytical model for these conditions are also shown in Fig. 13 and are obtained from Eqs. (25) by using the proper strain-rate values. It is seen from

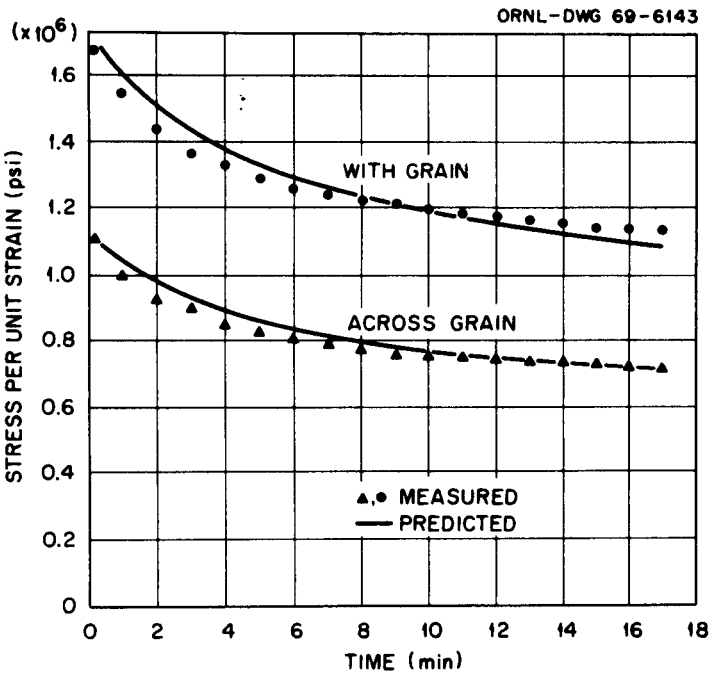

Fig. 11. RVD Stress Relaxation at 4500°F.

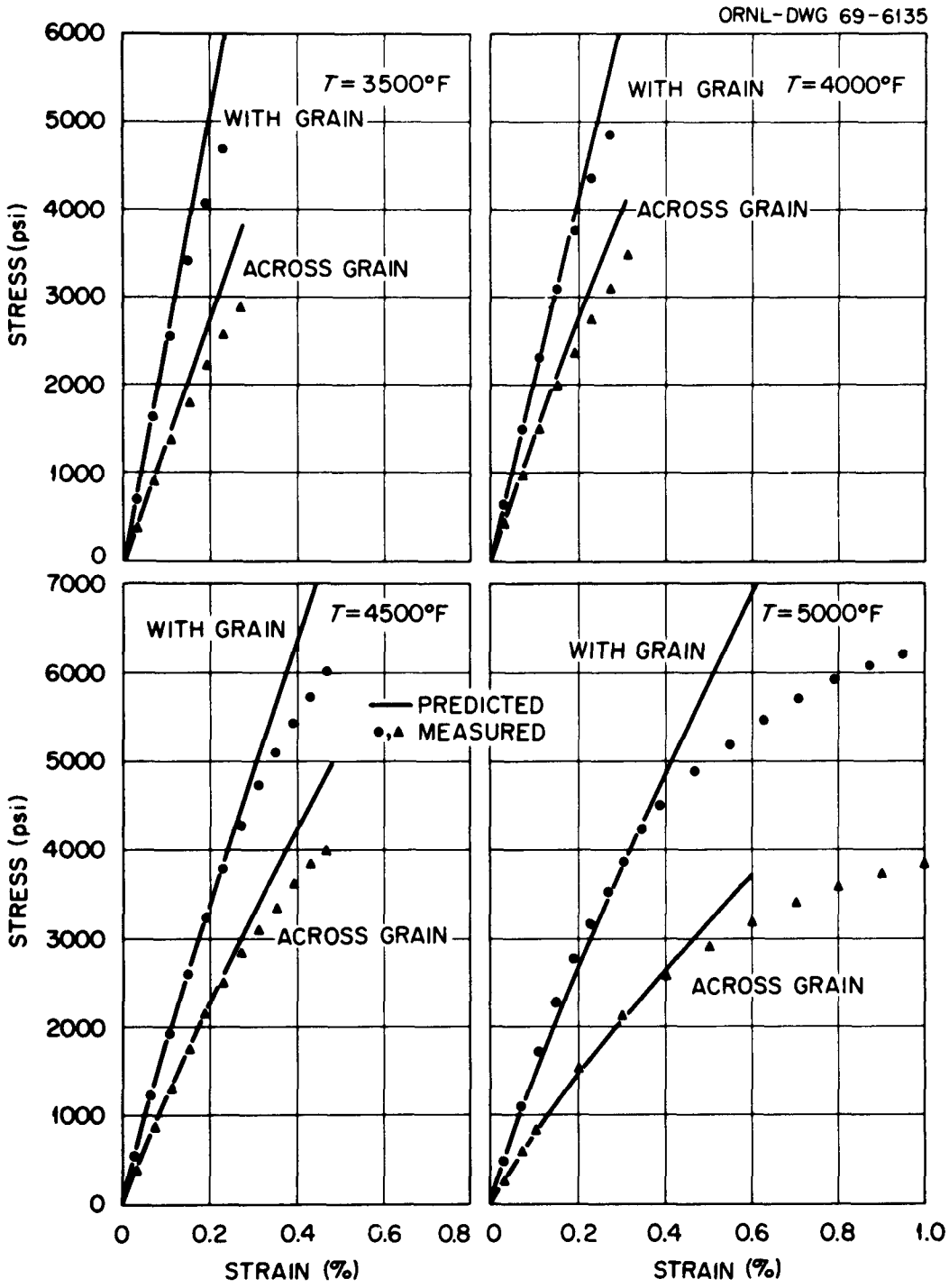

Fig. 12. Tensile Stress-Strain Curves for RVD Graphite.

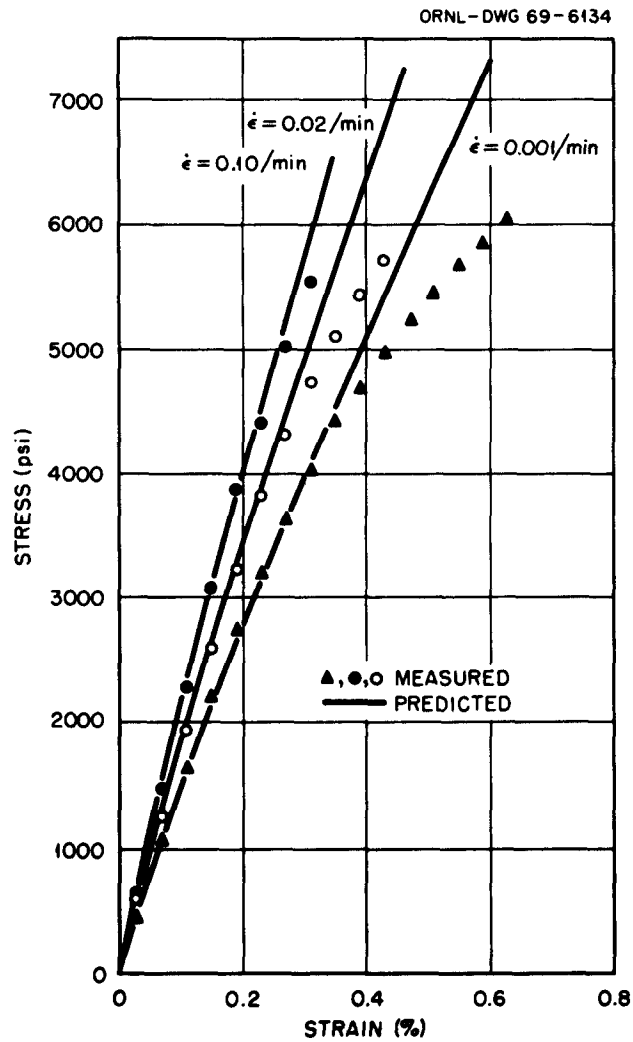

Fig. 13. Effect of Strain Rate on RVD With-Grain Tensile Stress-Strain Curves at 4500°F.

Fig. 13 that the strain-rate effect is predicted remarkably well by the viscoelastic model at this temperature and for the stress range to which the model is limited.

Both with-grain and across-grain compressive creep tests were conducted at 4500°F in a manner analogous to the tensile creep tests discussed earlier. Each of these compressive creep tests was performed with a uniaxial stress level equal to approximately 75% or 200% of the nominal ultimate tensile stress value, and therefore beyond the demonstrated range of applicability of the previously developed linear model. The ratios of creep strain after 20 minutes to applied stress for with-grain creep tests are plotted against the applied stress in Fig. 14. The tensile data shown previously in Fig. 2 are shown in addition to the compressive data. The compressive data appear to have the same general dependence on stress level as the tensile data. This is, therefore, an indication that the model presented in this report will likely apply for compressive conditions as long as the stresses are within the limited stress range defined earlier.

Conclusions

This study has shown that the time-dependent mechanical behavior of RVD graphite at temperatures ranging from 3500 to 5000°F can be represented over a limited stress range by a transversely isotropic linear viscoelastic model. For stress levels up to one-half of the nominal ultimate stress values, this model is shown to adequately predict uniaxial creep, relaxation, and stress-strain behaviors of both with-grain and across-grain specimens.

The experimental data used in this study allowed the complete evaluation of the viscoelastic model, except for the shear creep function $J_{44}(t)$ which describes the shear behavior in planes normal to the plane of isotropy. The model as developed, however, is sufficient to allow predictions which do not involve this type of shear behavior.

A temperature-dependent activation energy was associated with the steady-state creep coefficient. This energy varied from 106 kcal/mole at 3500°F to 228 kcal/mole at 5000°F. The temperature dependence of the

ORNL-DWG 69-13917

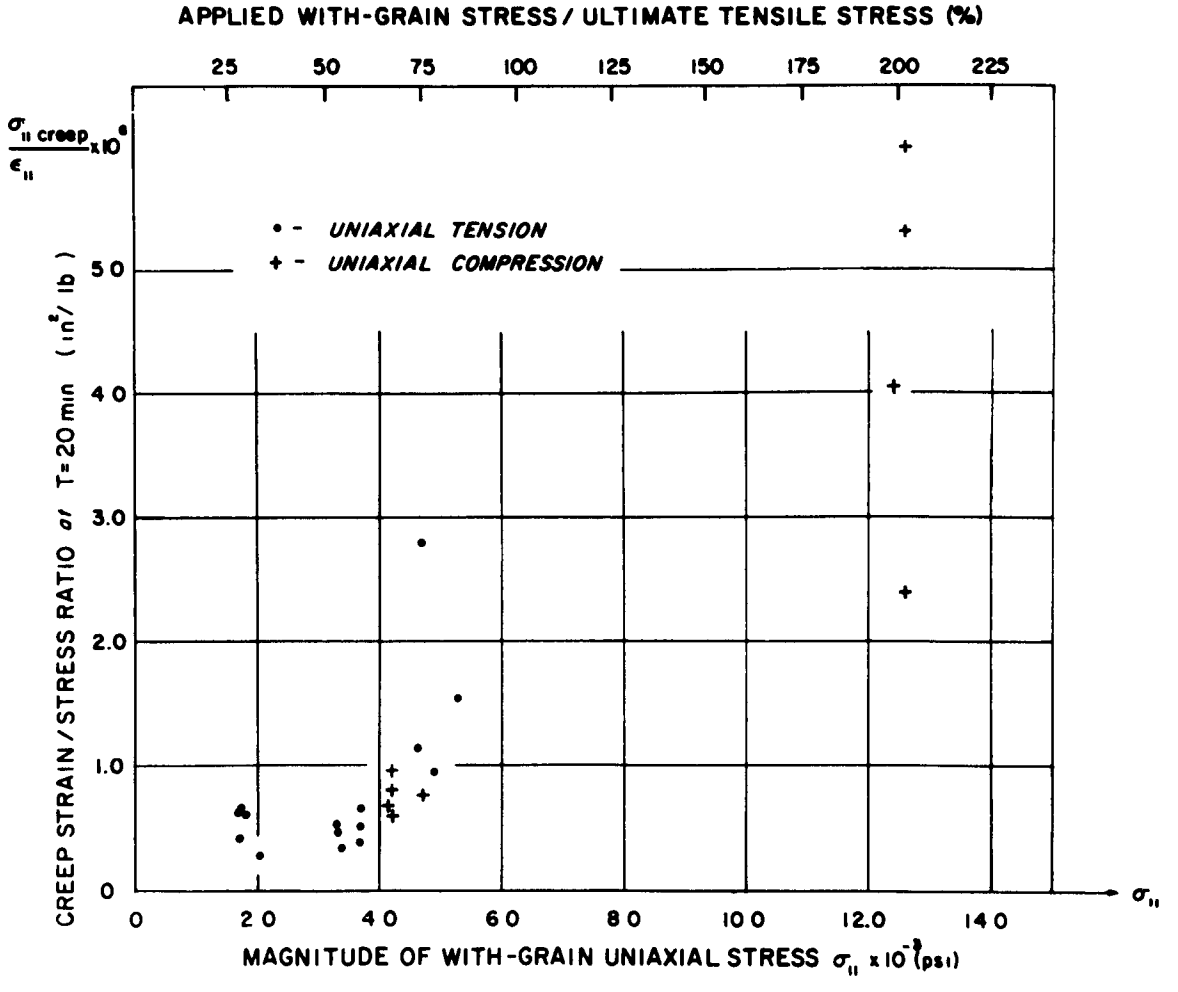

Fig. 14. With-Grain Creep Strain/Stress Ratio Versus Stress at 4500°F.

activation energy probably implies that more than one deformation mechanism is active in this temperature range. However, these activation energies seem to be in the range of activation energies for diffusion processes.[8]

The types of tests included in this study were diversified enough that some of the tests discussed were independent of the tests used to evaluate the parameters appearing in the constitutive equations. This allowed a completely independent comparison of model predictions with experimental measurements for these tests. Specifically, model predictions were compared with experimental results for across-grain creep tests, for with-grain and across-grain relaxation tests, and for short-time stress-strain tests conducted at various strain rates. The generally good correlation of analytical model predictions with experimental results indicates the capability of this model to predict the response of the material to more general loading conditions.

Acknowledgements

The author expresses his appreciation to B. L. Greenstreet and G. T. Yahr, Reactor Division of the Oak Ridge National Laboratory, for many helpful discussions during the course of this investigation.

References

1. W. N. Reynolds, Physical Properties of Graphite, Elsevier Publishing Co., Ltd., New York, 1968.

2. W. L. Greenstreet, "Mechanical Properties of Artificial Graphites — A Survey Report," USAEC Report ORNL-4327, Oak Ridge National Laboratory, December 1968.

3. J. D. Woodard, "An Investigation of the Mechanical Behavior of Grades RVD and AGOT Graphites, Final Report," USAEC Report TID-23288, Southern Research Institute, April 20, 1966.

4. Wilhelm Flügge, Viscoelasticity, Blaisdell Publishing Co., Waltham, Massachusetts, 1967, pp. 24-30.

5. T. G. Rogers and A. C. Pipkin, "Asymmetric Relaxation and Compliance Matrices in Linear Viscoelasticity," Zeitschrift für angewandte Mathematik and Physik, 14: 334-343 (1963).

6. R. E. Nightingale, Nuclear Graphite, Academic Press, New York, 1962, pp. 90-91.

7. R. L. Woolley, "The Yield Curve and Compressive Strength of Polycrystalline Graphite," The Philosophical Magazine, 11(112): 799-807 (1965).

8. M. A. Kanter, "Diffusion of Carbon Atoms in Natural Graphite Crystals," Physical Review, 107(3): 655-663 (1957).

This page left intentionally blank

Internal Distribution

1. S. E. Beall
2. H. W. Behrman, RDT
3. M. Bender
4. E. S. Bettis
5. H. W. Blake (Y-12)
6. S. E. Bolt
7. J. W. Bryson
8-12. J. P. Callahan
13. S. J. Chang
14. W. H. Cook
15. J. M. Corum
16. W. B. Cottrell
17. F. L. Culler
18. R. W. Derby
19. W. G. Dodge
20. W. P. Eatherly
21. A. P. Fraas
22-31. B. L. Greenstreet
32. R. C. Gwaltney
33. D. G. Harman
34. P. N. Haubenreich
35. P. R. Kasten
36. C. R. Kennedy
37. K. C. Liu
38. M. I. Lundin
39. R. N. Lyon
40. H. G. MacPherson
41. R. E. MacPherson
42. H. E. McCoy
43. H. C. McCurdy
44. G. B. Marrow (Y-12)
45. J. G. Merkle
46. A. J. Miller
47-48. S. E. Moore
49. J. M. Napier (Y-12)
50. H. A. Nelms
51. A. M. Perry
52. T. W. Pickel
53-67. C. E. Pugh
68. J. N. Robinson
69. M. W. Rosenthal
70. W. K. Sartory
71. A. W. Savolainen
72. Dunlap Scott
73. M. J. Skinner
74. J. E. Smith
75. I. Spiewak
76. J. L. Spoormaker
77. D. A. Sundberg
78. R. W. Swindeman
79. D. B. Trauger
80. R. S. Valachovic
81. M. S. Wechsler
82. J. R. Weir
83. G. D. Whitman
84-85. G. T. Yahr
86. Gale Young
87-88. Central Research Library
89-90. Y-12 Document Reference Section
91-95. Laboratory Records Department
96. Laboratory Records, ORNL R.C.

External Distribution

97. H. W. Babel, Douglas Aircraft Co., Santa Monica, Calif.
98. J. C. Bokros, Gulf General Atomic, San Diego, Calif.
99. S. A. Bortz, IIT Research Institute, Chicago
100. H. L. Brammer, SNPO-C, NASA Lewis Research Center, Cleveland
101. L. C. Corrington, SNPO-C, NASA Lewis Research Center, Cleveland
102. H. T. Corten, University of Illinois, Urbana, Ill.
103. J. F. Cully, SNPO-A, c/o USAEC, P. O. Box 5400, Albuquerque
104. R. J. Dietz, Los Alamos Scientific Laboratory
105. A. J. Edmondson, The University of Tennessee, Knoxville
106. R. P. Felgar, TRW Systems, Redondo Beach, Calif.
107. D. B. Fischbach, Jet Propulsion Laboratory, Pasadena, Calif.
108. D. M. Forney, Air Force Materials Laboratory (MAC), Wright-Patterson Air Force Base, Ohio

109. C. W. Funk, Aerojet-General Corp., Sacramento, Calif.
110. J. J. Gangler, Materials Engineering Branch, RRM, NASA, Washington
111. W. V. Green, Los Alamos Scientific Laboratory
112. E. D. Gurley, North Carolina State University, Raleigh, N.C.
113. Harold Hessing, SNPO-A, CMB Div., Los Alamos Scientific Lab.
114. A. N. Holden, Westinghouse Astronuclear Laboratory, Pittsburgh
115. L. E. Hulbert, Battelle Memorial Institute, Columbus, Ohio
116. J. R. Hunter, USAEC, Washington, D.C.
117. Gary Kaveny, Aerojet-General Corp., Sacramento, Calif.
118. B. T. Kelley, UKAEA, Culcheth, Warrington, Lancashire, England
119. W. V. Kotlensky, Raytheon Co., Waltham, Mass.
120. J. J. Krochmal, Air Force Materials Laboratory, Wright-Patterson Air Force Base, Ohio
121. J. J. Lombardo, SNPO-C, NASA Lewis Research Center, Cleveland
122. H. H. W. Losty, The General Electric Co., Ltd., HIRST Research Centre, Wembley, England
123. L. L. Lyon, Los Alamos Scientific Laboratory
124. D. P. MacMillan, Los Alamos Scientific Laboratory
125. M. M. Manjoine, Westinghouse Astronuclear Laboratory, Pittsburgh
126. H. E. Martens, Jet Propulsion Laboratory, Pasadena, Calif.
127. J. L. Mershon, USAEC, Washington, D.C.
128. J. E. Morrissey, USAEC, Washington, D.C.
129. R. E. Nightingale, Pacific-Northwest Laboratory, Richland
130. E. T. Onat, Yale University, New Haven, Conn.
131. C. D. Pears, Southern Research Institute, Birmingham, Ala.
132. Hui Pih, The University of Tennessee, Knoxville
133-134. D. L. Platus, Mechanics Research, Inc., El Segundo, Calif.
135. J. W. Prados, The University of Tennessee, Knoxville
136. W. G. Ramke, Air Force Materials Laboratory, Wright-Patterson Air Force Base, Ohio
137. J. R. Richardson, SNPO-C, NASA Lewis Research Center, Cleveland
138-139. J. C. Rowley, Los Alamos Scientific Laboratory
140. W. S. Scheib, SNPO, USAEC, Washington, D.C.
141. R. W. Schroeder, SNPO-C, NASA Lewis Research Center, Cleveland
142. F. C. Schwenk, SNPO, USAEC, Washington, D.C.
143. E. J. Seldin, Parma Research Center, Cleveland
144. R. H. Singleton, Westinghouse Astronuclear Laboratory, Pittsburgh
145. M. C. Smith, Los Alamos Scientific Laboratory
146. G. B. Spence, Parma Research Center, Cleveland
147. H. S. Starrett, Southern Research Institute, Birmingham, Ala.
148. J. L. Swanson, Westinghouse Astronuclear Laboratory, Pittsburgh
149. R. D. Snyder, West Virginia University, Morgantown, W. Va.
150. N. R. Thielke, SNPO, NASA Lewis Research Center, Cleveland
151. Tu-Lung Weng, Parma Research Center, Cleveland
152. E. G. Zukas, Los Alamos Scientific Laboratory
153-167. Division of Technical Information Extension (DTIE)
168. Laboratory and University Division, ORO